ChemPubSoc Europe

DOI: 10.1002/cphc.201600692

CHEMPHYSCHEM Articles

Ion Dynamics in a Mixed-Cation Alkoxy-Ammonium Ionic Liquid Electrolyte for Sodium Device Applications

Cameron R. Pope,[a] Mega Kar,[b, c] Douglas R. MacFarlane,[b, c] Michel Armand,[a, d] Maria Forsyth,[a, c] and Luke A. O'Dell*[a]

The ion dynamics in a novel sodium-containing room-temperature ionic liquid (IL) consisting of an ether-functionalised quaternary ammonium cation and bis(trifluoromethylsulfonyl)-amide [NTf_2] anion with various concentrations of Na[NTf_2] have been characterised using differential scanning calorimetry, impedance spectroscopy, diffusometry and NMR relaxation measurements. The IL studied has been specifically designed to dissolve a relatively large concentration of Na[NTf_2] salt (over 2 mol kg^{-1}) as this has been shown to improve ion transport and conductivity. Consistent with other studies, the measured ionic conductivity and diffusion coefficients show that the overall ionic mobility decreases with decreasing temperature and increasing salt content. NMR relaxation measurements provide evidence for correlated dynamics between the ether-functionalised ammonium and Na cations, possibly with the latter species acting as cross-links between multiple ammonium cations. Finally, preliminary cyclic voltammetry experiments show that this IL can undergo stable electrochemical cycling and could therefore be potentially useful as an electrolyte in a Na-based device.

1. Introduction

Society's growing dependence on portable and large-scale energy storage devices has increased the demand for high-energy-density and higher-capacity, environmentally conscious electrochemical storage technologies. This demand stems from the need for load-levelling of intermittent renewable energy technologies, such as solar and wind electricity generation, both at the household and neighbourhood level and also at the grid level.[1] These medium- to large-scale applications require significant advances in cost and safety aspects of traditional Li-ion technology and these issues have directed many research groups to investigate the viability of sodium electrochemistry as an alternative to lithium, and ionic liquids (ILs) as an alternative to carbonate electrolytes.[2]

[a] C. R. Pope, Prof. M. Armand, Prof. M. Forsyth, Dr. L. A. O'Dell
Institute for Frontier Materials (IFM)
Deakin University
Waurn Ponds, Geelong, Victoria 3216 (Australia)
E-mail: luke.odell@deakin.edu.au

[b] Dr. M. Kar, Prof. D. R. MacFarlane
School of Chemistry
Monash University
Clayton 3800, Victoria (Australia)

[c] Dr. M. Kar, Prof. D. R. MacFarlane, Prof. M. Forsyth
ARC Centre of Excellence for Electromaterials Science (ACES)
Institute for Frontier Materials (IFM)
Deakin University
Burwood, Victoria 3125 (Australia)

[d] Prof. M. Armand
CIC EnergiGUNE
Parque Tecnólogico de Álava
Albert Einstein 48 Edificio CIC
01510, Miñano, Álava (Spain)

The ORCID identification number(s) for the author(s) of this article can be found under http://dx.doi.org/10.1002/cphc.201600692.

ILs have established themselves as a class of compounds that can be tailored to a vast number of applications. The advantages of ILs over traditional solvent-based electrolytes pertains to the ability to design systems with negligible vapour pressure, lack of volatility, high ionic conductivity and good thermal and electrochemical stability.[2–4] Some ILs also possess a wide electrochemical window, which is highly advantageous for electrochemical applications, specifically for batteries, supercapacitors and fuel cells.[5–6]

The primary reason for the expanding interest in sodium-based devices lies in the high abundance and potentially lower manufacturing costs of these devices in comparison to lithium,[,6–8] combined with the shortfall of lithium resources and the push for more widely adopted renewable energy transportation. While lithium systems have been studied for several decades and are the most commercialised mobile battery technology, the identification of suitable sodium intercalating electrodes and sodium electrolytes that demonstrate stable cycling is needed before sodium devices can be considered a viable alternative to lithium. Whilst both the electrode and electrolyte, as well as the interface between these, must be optimised, here we will focus on the transport properties of the electrolyte.

Though the field is still very much in its infancy, recent publications detailing sodium-conducting organic solvent,[9–10] polymer[11–13] and ionic liquid[14–17] electrolytes have demonstrated the viability of sodium devices. The use of IL electrolytes has proven to be useful in particular for Na-metal-based devices, as they can negate the Na-anode corrosion issue observed in commonly used organic carbonate electrolytes, which result in unstable cycling as the sodium metal is consumed.[18] Recently, Singh et al.[19] have reported the higher stability of the passiva-

tion layer formed on the aluminium current collector up to 5 V at 328 K afforded by Na bis(fluorosulfonyl)imide (Na[FSI]) in C_3mpyr[FSI], which overcomes the additional restriction formerly imposed by the corrosion of the Al collector.

While many sodium-based electrolytes may be expected to behave similarly to their lithium analogues, there will be differences in the coordination environment, transport properties and ion solvation. One of these differences was demonstrated by Monti et al.[14] who focused on the interactions in 1-ethyl-3-methylimidazolium bis(trifluoromethylsulfonyl)amide (EMIm[NTf_2]) as a function of Na[NTf_2] salt concentration, in which the charge carrier was found to be $[Na[NTf_2]_3]^{2-}$, in contrast to the $[Li[NTf_2]_2]^-$ for the lithium analogue. Recent work by Fukunaga et al.[20] demonstrated a more traditional molten salt eutectic mixture of Na[FSI]-K[FSI], showing stable cycling performance while operating between 333–363 K, while ILs such as the Na[FSI]-C_3mpyr[FSI] and Na[NTf_2]-$C_n$mpyr[NTf_2] systems reported by Ding et al.,[15–16] Noor et al.,[17,21] Yoon et al.[22–23] are considered to be more advantageous due to the lower operating temperature, where sodium cells can be cycled from 298–373 K. Ding et al.[15] demonstrated a 2:8 molar ratio of Na/Na[FSI] C_3mpyr[FSI]/$NaCrO_2$ cell with a coulombic efficiency in excess of 99% when cycled over various C rates at 353 K.

Interestingly, at higher Na salt concentrations in ILs, the electrochemical performance for Na metal cycling seems to be improved despite lower overall ionic conductivities.[23] This is attributed to decreased electrode surface impedance, indicative of multiple ion transport mechanisms, and the relatively large concentration of Na ultimately resulting in enhanced Na ion transport numbers. Indeed, Hagiwara et al.[16] showed a full working device with excellent capacity and rate capability for a 40 mol% Na[FSI] salt in C_3mpyr[FSI] IL. These high salt concentration systems were also shown to behave well for equivalent lithium metal devices[24] in which a 3.2 mol kg^{-1} concentration (1:1 molar ratio) of Li[FSI] was successfully cycled, demonstrating high rate charge and discharge characteristics. The $[FSI]^-$ anion seems to be a key in achieving higher salt concentrations in those ILs

Another approach to increasing salt concentration in the electrolyte, even without using the $[FSI]^-$ anion, may be to incorporate a strong solvating group that could coordinate the Na ion and hence increase solubility. Ether functionality may be one approach to achieve this, as will be shown in the present work. Watanabe et al.[25] have previously demonstrated the lithium chelating ability of equimolar mixtures of glymes in the Li[NTf_2] salt and have discussed the strong coordination observed between alkali metal cations and strong Lewis bases, such as ethers. It was observed that a weak Lewis-acidic cation, such as the lithium–glyme complex, and a weak Lewis-basic anion leads to ionic dissociation. They have also studied an equimolar mixture of pentaglyme (G5) and Na[NTf_2] in which the high ionicity suggested the solvate IL dissociates into the separate sodium glyme complex $[Na(G5)]^+$ cation and $[NTf_2]^-$ anion, despite the extremely high salt concentration in the liquid.[26] Kar et al.[27–28] made a similar observation where a novel quaternary alkoxy bis(trifluoromethylsulfonyl)amide [NTf_2] based IL with multiple oligo-ether side chains was demonstrated to interact and successfully solubilise zinc ions in an electrolyte proposed for a Zn-air battery system.

Building on this knowledge, the quaternary ammonium trialkoxy $[N_{2(20201)(20201)(20201)}][NTf_2]$ system, which was previously synthesised and investigated for Zn based systems, is explored here for Na-ion based electrolytes. Rather than a single triglyme or tetraglyme type side chain on the nitrogen, the increase in ether functionality is achieved through multiple shorter-chain glyme substituents which may somewhat negate the chelating effect previously observed for Zn.[29] In order to determine the viability of this Na-ion-based IL electrolyte, we have utilised ^1H, ^{19}F and ^{23}Na NMR spin-lattice (T_1) relaxation measurements and ^1H and ^{19}F PFG NMR diffusion experiments to elucidate the ion dynamics and speciation in this system as a function of Na concentration and temperature. Additionally, we have carried out preliminary cyclic voltammetry experiments that demonstrate this system's promising Na electrochemical behaviour and good potential for use as an electrolyte in a Na ion battery.

Experimental Section

Sample Preparation

The *N*-ethyl-2-(2-methoxyethoxy)-*N*,*N*-bis(2-(2-methoxyethoxy) ethyl) ethan-1-aminium ($N_{2(2O2O1)(2O2O1)(2O2O1)}$) bis(trifluoromethylsulfonyl)amide (NTf_2) IL (see Figure 1) was synthesised according to literature procedures.[29] Various concentrations of the sodium-based IL were prepared by mixing with sodium bis(trifluoromethylsulfonyl)amide, Na[NTf_2] (99.9%, Solvionics™).

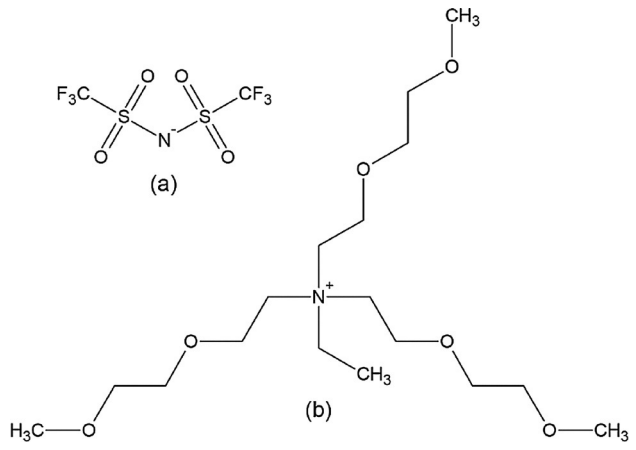

Figure 1. Structure of a) the NTf_2 anion and b) ether-functionalised quaternary ammonium cation used in this study.

Solubility tests indicated a maximum possible Na[NTf_2] concentration in this IL of 2.16 mol kg^{-1} at 298 K corresponding to a molar ratio of 57% sodium. Four electrolyte concentrations were prepared for characterisation, namely 0.2, 0.5, 1.0 and 2.0 mol kg^{-1} Na[NTf_2]. Due to the similarities in results between the 2.0 mol kg^{-1} and the 2.16 mol kg^{-1} concentrations, the 2.16 mol kg^{-1} has been excluded from this work. Samples were stored and handled under the protection of a high-purity argon atmosphere and dried in

a vacuum oven at 353 K for 48 hours prior to commencing characterisation to ensure a water content <200 ppm, as determined by Karl Fischer titration (Metrohm).

Differential Scanning Calorimetry

Thermal analysis was conducted on a liquid nitrogen equipped Mettler Toledo DSC 1 STAR differential scanning calorimeter (DSC), where 8 to 15 mg of sample was hermetically sealed in a 40 μL aluminium pan. Calibration of the instrument was completed using a cyclohexane standard for sub-ambient temperatures and indium for high temperatures. Three consecutive temperature scans of the sample were conducted prior to data acquisition to ensure thermal stability of the sample and negate any instances of thermal hysteresis. A steady flow of inert nitrogen gas was supplied to the instrument in order to preserve a dry environment inside the experimental chamber. Thermograms were recorded on both heating (123–473 K) and cooling (473–123 K) cycles at a scan rate of 10 K min^{-1}. Mettler Toledo STAR^e (v 10.0) and OriginPro (v 8.5.1) software were utilised to perform data analysis and to extract glass transition temperatures (T_g) for the samples, which are reported as the mid-point of the heat-capacity change on the heating scan (Section 2.2).

Electrochemical Impedance Spectroscopy

Electrochemical impedance spectroscopy (EIS) measurements were conducted on a single-channel Bio-Logic SP-200 potentiostat equipped with a low-current cable using EC-Lab (v10.38) software (Bio-Logic Scientific Instruments). A platinum wire electrode conductivity cell that was calibrated at 298 K using 0.01 M KCl solution was used for the measurements. Samples were sealed into the conductivity cell and Teflon tape was used to ensure an inert environment inside the cell. A 0.1 V AC potential (100 μV resolution) was used over a frequency range from 0.1 Hz to 1 MHz. Measurements were conducted over a temperature range from 298–353 K in 10 K increments to observe any instances of hysteresis upon heating and cooling. The cell temperature was controlled to within ± 0.2 K using a brass block heater with a T-type thermocouple attached to a Eurotherm 2204e temperature controller. A 15 min delay was used after each temperature step to ensure thermal homogeneity of the sample prior to data acquisition. Data analysis was conducted using OriginPro (v8.5.1) software in conjunction with EC-Lab (v10.38) software to determine the conductance from the impedance measurements.

Nuclear Magnetic Resonance Spectroscopy

Samples were loaded into 5 mm Duran type-E NMR tubes and a sealed D_2O capillary was inserted before the 5 mm tube was sealed with a high-temperature Teflon cap and Teflon tape. All ^{1}H and ^{19}F experiments were performed at a magnetic field strength of 7.05 T (^{1}H Larmor frequency of 300 MHz) on a Bruker Avance III 300 MHz wide-bore spectrometer, using a 5 mm Bruker Diff50 pulse-field gradient probe with a maximum gradient strength of 2500 G cm^{-1}. The ^{23}Na relaxation measurements were carried out at 11.7 T on a Bruker Avance III 500 MHz wide-bore spectrometer and a 5 mm static probe.

Sample temperatures were calibrated using the ^{1}H signal from an aqueous solution of ethylene glycol (^{1}H and ^{19}F measurements) and the $^{[207]}$Pb signal from solid lead nitrate (^{23}Na measurements) and were controlled to within ± 0.1 K using a Bruker BCU over a temperature range of 263–353 K. An equilibration time of 15 min was used to ensure thermal homogeneity across the sample prior to conducting each measurement. Temperatures below 273 K were obtained using a liquid nitrogen evaporator.

Pulsed-Field Gradient Diffusometry

The temperature-dependent diffusion coefficients (D) were obtained for the ^{1}H and ^{19}F nuclei as these have proven to be invaluable for the analysis of molecular transport in ILs.[30] The ^{1}H nuclei were used to probe the bulky alkyl ammonium cation due to the absence of protons within the inorganic anion. As ^{19}F is only present in the anion, this allowed for D_{cation} and D_{anion} to be resolved. The diffusion coefficients for the ^{23}Na nuclei were unable to be obtained due to the combination of short ^{23}Na T_2 relaxation times and gradient strength limitations. The pulsed field gradient stimulated echo (PFG-STE) pulse sequence was utilised with the magnitude of the applied gradient varied in 16 increments and the maximum gradient strength, gradient pulse length and diffusion time (Δ) optimised in each case. The ^{1}H 90° pulse length was 9.5 μs and recycle delays were set to $>5T_1$ in all cases. Convection effects at higher sample temperatures were minimised by inserting a smaller capillary containing D_2O into the NMR tube containing the IL to provide a physical barrier to the convective flow. Additionally, repeat measurements were made with the diffusion time Δ varied and D extrapolated to $\Delta = 0$. The data were fitted to the Stejskal–Tanner equation [Eq. (1)] using a non-linear least-squares method within the Bruker TopSpin software (v3):

$$I = I_0 \exp\left[-D\gamma^2 g^2 \delta^2 \left(\Delta - \frac{\delta}{3}\right)\right] \quad (1)$$

In this expression, I is the observed signal intensity, I_0 is the maximum signal intensity, γ is the gyromagnetic ratio of the nucleus being observed, g is the gradient strength and δ is the gradient pulse duration.

Spin-Lattice (T_1) Relaxation Measurements

Spin-lattice (T_1) relaxation measurements were conducted to probe the short timescale dynamics of the both the sodium and IL cation and anion. This was achieved by probing the ^{1}H, ^{19}F and ^{23}Na nuclei at 300, 282 and 132 MHz, respectively. The ^{1}H T_1 measurements were conducted using a saturation recovery solid-echo pulse sequence with an echo delay of 20 μs and 16 relaxation delays varying from 5 ms to 10 s. The ^{23}Na T_1 values were obtained using the inversion recovery sequence with a 12 μs 180° pulse length and 16 relaxation delays over the time period from 1 μs–100 ms. ^{19}F measurements also used the inversion recovery sequence with 21 relaxation delays varying from 1 μs −2 s. Recycle delays were set to $>5T_1$ for the latter experiments.

Cyclic Voltammetry

Cyclic voltammetry (CV) data provides an indication of the reversibility, stability and ultimately the viability of the electrochemical reactions present in a device.[23] The experimental setup consisted of a 1.5 mm diameter copper working electrode, a coiled platinum counter electrode and a platinum reference electrode. Potentials were checked with a $Fc|Fc^+$ internal reference. CV measurements were conducted at 323 K and 348 K using a 10 mV s^{-1} scan rate.

2. Results and Discussion

2.1. Sodium Solubility

The highest Na[NTf_2] concentration achieved for this IL was a substantial 2.16 mol kg^{-1}, equating to a Na concentration of 57 mol%. This is a relatively high concentration in comparison to other systems. Reported Na salt concentrations in other ILs include 0.75 mol kg^{-1} [31], 0.8 mol kg^{-1} in the mixed-anion system Na[NTf_2] in C_3mpyr[FSI] as reported by Ding et al.[15], 1.35 mol kg^{-1} in C_3mpyr[FSI] by Yoon et al.[22] and as much as 60 mol% Na[FSI] in C_3mpyr[FSI] by Hagiwara et al.,[16] though they later found that 40 mol% Na[FSI] achieved the highest rate capability at 363 K with the optimum concentration demonstrated to be the 25 mol% concentration below ambient temperatures.

2.2. Thermal Analysis

The addition of Na[NTf_2] to the IL saw a marked increase in T_g by 53 K when comparing the neat IL to the 2.0 mol kg^{-1} sample (see Figure 2 and Table 1). An increase in T_g is always observed upon adding either Li or Na salts to ILs,[22,32] however it is more prominent here in these high-concentration, ether-containing ILs. As T_g is a qualitative measure of the ion mobility[33] it can be assumed that this increase, which also corresponds to an increase in apparent viscosity, is related to a higher degree of ion–ion interactions at higher salt concentrations.[33] As a result, based on this data, the ionic conductivity would be expected to decrease with increasing Na salt concentration, as discussed in Section 2.3. Significant endothermic peaks (T_g overshoot) are also notable at lower salt concentrations. Such enthalpy overshoot is a kinetic phenomenon often observed in polymers undergoing structural relaxation near the T_g,[34–35] and can be attributed to the rapid increase in the free volume and molecular disorder near T_g.

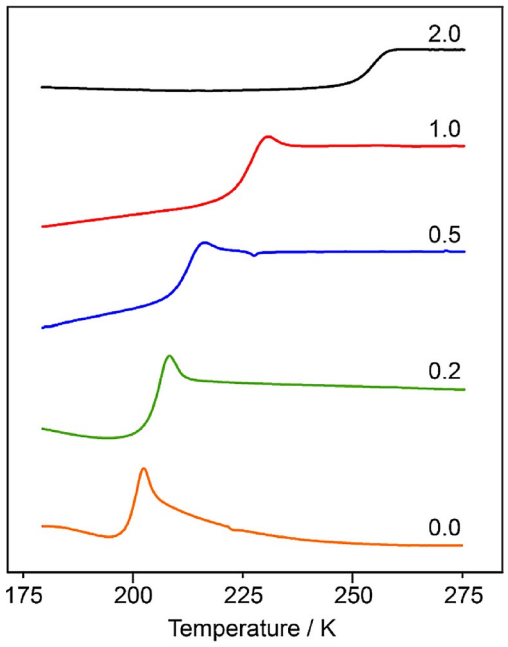

Figure 2. DSC thermograms obtained from the ionic liquid containing the concentrations of $NaNTf_2$ as indicated (mol kg^{-1}).

Table 1. VTF fitting parameters [Eq. (2)] obtained from the variable temperature ionic conductivity data, and glass transition temperatures extracted from the DSC traces for the ionic liquid with various $NaNTf_2$ concentrations.

$NaNTf_2$ concentration [mol kg^{-1}]	σ_0 [S cm^{-1}]	B [K]	T_0 [K]	T_g[K] (midpoint)	T_g [K] (onset)
0.0	0.09 ± 0.10	310 ± 150	230 ± 30	201	196
0.2	0.15 ± 0.20	520 ± 150	205 ± 15	203	197
0.5	0.23 ± 0.20	710 ± 200	192 ± 20	212	207
1.0	0.25 ± 0.30	775 ± 300	198 ± 20	229	218
2.0	3.2 ± 4.0	1625 ± 400	165 ± 15	254	246

2.3. Ionic Conductivity

The measured ionic conductivities for the pure IL and various concentrations of Na[NTf_2] are presented in Figure 3. The highest conductivity was observed in the pure IL sample with a conductivity of 6.56×10^{-3} at 348 K. While all the Na[NTf_2] concentrations demonstrated high ionic conductivities at elevated temperatures, the conductivities across the entire measured temperature range decrease with increasing Na[NTf_2] content. As the Na content increases, in addition to the reduction in free volume, which will hinder both rotational and translational dynamics, a further effect due to the enhanced ion associations may be expected; Na will be highly coordinated by the anions as well as the alkoxy groups on the ammonium cation, which may also result in cross-linking between multiple IL cations.

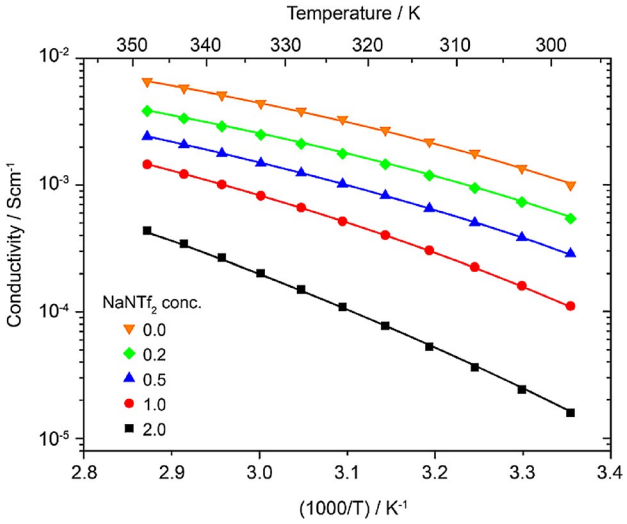

Figure 3. Ionic conductivity of the IL as a function of inverse temperature for various $NaNTf_2$ concentrations as indicated (mol kg^{-1}). Lines show VTF fits [Eq. (2)]. The error bars are contained within the size of the data points.

The conductivities of all samples demonstrated non-Arrhenius behaviour, and were fitted to the Vogel–Tammann–Fulcher (VTF) equation [Eq. (2)] using least-squares curve-fitting (Table 1):

$$\sigma = \sigma_0 e^{-B/(T-T_0)} \quad (2)$$

In this expression, σ_0 is the pre-exponential conductivity factor (the conductivity at infinite temperature), B is a pseudo activation energy and T_0 is closely related to the glass transition temperature and indicates the temperature at which free volume and mobility is reduced to zero.[36]

The parameters extracted from the VTF fits are presented in Table 1. Due to the limited temperature range and the slight curvature of the data sets, the associated uncertainties in these parameters are rather large. Nonetheless, some trends are apparent. As expected, the T_0 values in all cases are less than or equal to the glass transition temperature T_g (to within the uncertainty of the fit). However, whereas the T_0 value should track T_g, in this system, the T_0 decreases whilst the T_g substantially increases, resulting in a greater T_g-T_0 value at the highest concentrations of Na[NTf_2]. Even accounting for the uncertainty in the fits, the addition of 2.0 mol kg^{-1} of Na[NTf_2] to the pure IL leads to a T_g-T_0 value of 90 compared to around 30 °C for the other systems. As T_0 is an arbitrary constant subtracted from T_g with an empirical approximation of $T_0-T_g \approx 50$ K for ILs,[37] such a large value for T_g-T_0 is suggestive of decoupling of the conductivity from T_g and the onset of some level of ionic mobility at temperatures below the glass transition. Such an effect can be better visualised in a plot of the ionic conductivities versus T/T_g (Figure 4), wherein the data sets for the two highest concentrations are located further to the left.

As discussed above, the observation of higher T_g values as the salt concentration increases is typical in ILs, and is also consistent with the decreasing ionic conductivities. While the pre-exponential conductivity values (σ_0) appear to increase with salt concentration, they have rather large associated uncertainties and in fact stay approximately consistent within this range, while the pseudo activation energies (B) increase significantly, in particular for the highest salt concentration. The latter effect would be expected to arise in the case of associations between the Na^+ and IL cations, which would affect the mobility of both species. Despite the higher T_g, the relatively high conductivity suggests that at these high salt concentrations, the mechanism for cation motion is modified in comparison with the more typical, lower concentration systems, and this can have a positive impact on the Na transport number, as has been shown previously.[23,38] Therefore, the high Na salt concentrations achieved in this system have the potential to perform well in electrochemistry applications. Indeed, the measured ionic conductivity does not necessarily correlate to optimum device performance,[39] and often electrolytes with higher salt concentrations perform better despite lower conductivity values. Detailed electrochemical studies of these ILs are currently underway to investigate this and will be reported in detail in a future publication. However, some preliminary cyclic voltammograms are presented in Section 2.6.

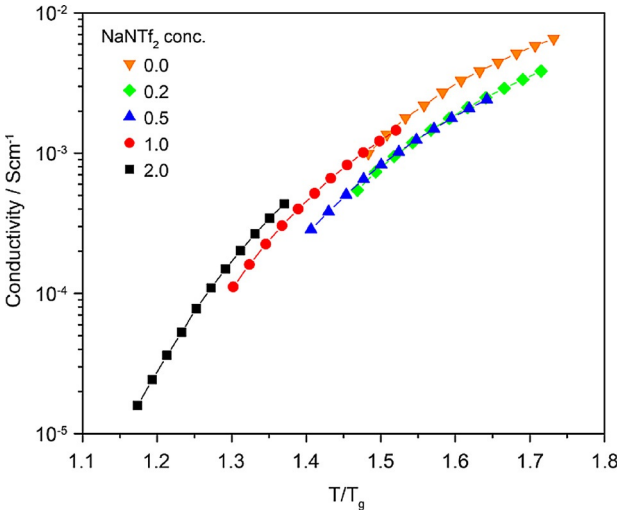

Figure 4. Ionic conductivity versus T/T_g for the ionic liquid with $NaNTf_2$ concentrations indicated (mol kg^{-1}). The error bars are contained within the size of the data points.

2.4. Diffusion Measurements

^{1}H diffusion coefficients obtained as a function of temperature and Na[NTf_2] concentration are presented in Figure 5. As protons are only present in the [$N_{2(2O2O1)3}$] cation, these measurements quantify the IL cation diffusion. These diffusion coefficients exhibit similar behaviour to that observed for the ionic conductivities (Figure 3), in which increasing Na[NTf_2] concentrations result in reduced mobility. The approximately two orders of magnitude difference between the pure IL and the 2.0 mol kg^{-1} Na[NTf_2] diffusion coefficients again indicates the presence of strong associations between the IL cations and Na ions that reduce the overall translational mobility of the former

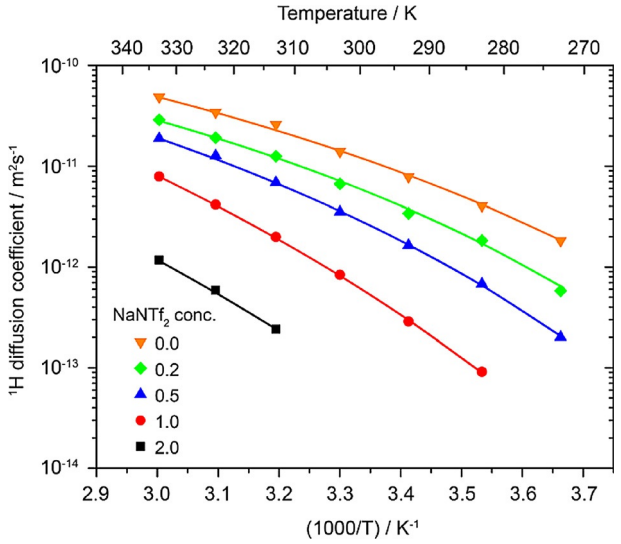

Figure 5. ^{1}H diffusion coefficients as a function of inverse temperature, with VTF fits shown [Eq. (2)] for all samples, except the highest $NaNTf_2$ concentration which shows a linear fit. Diffusion coefficients for this concentration below 310 K were below the detection limit. The error bars are contained within the size of the data points.

species. Also consistent with the conductivity data, the temperature dependence of the IL cation diffusion coefficients show a departure from Arrhenius behaviour with a noticeable curvature, and so were fitted to the VTF equation using the parameters shown in Table 2. Although the uncertainties are relatively large once again, the B and T_0 values obtained from these IL cation diffusion coefficients are equal to those obtained from the conductivity data to within the uncertainties of the fits, and thus the same trends are observed, with the pseudo activation energy increasing significantly at higher salt concentrations. The pre-exponential factors in this case (D_0, or the diffusion coefficients at infinite temperature) have lower relative uncertainties than for the conductivity fits, and are seen to decrease with increasing $Na[NTf_2]$ concentrations, once again consistent with a significant reduction in cation mobility.

Table 2. VTF fitting parameters [Eq. (2)] for the ^{1}H diffusion coefficients as measured by PFG-NMR.

$NaNTf_2$ concentration [mol kg^{-1}]	D_0 [m^{2}s^{-1}]	B [K]	T_0 [K]
0.0	$(8.0\pm5)\times10^{-9}$	765 ± 500	182 ± 30
0.2	$(5.2\pm4)\times10^{-9}$	730 ± 200	192 ± 30
0.5	$(1.1\pm0.5)\times10^{-8}$	910 ± 200	189 ± 30
1.0	$(1.3\pm0.9)\times10^{-7}$	1540 ± 300	175 ± 30

The anion diffusivities were also measured for selected $Na[NTf_2]$ concentrations via ^{19}F PFG NMR, and these are shown in Figure 6. They are higher than the cation diffusivities over the entire temperature and concentration range studied, which would be expected given the smaller molecular volume of the $[NTf_2]^-$ anion. The trend of decreasing diffusion coefficients as the $Na[NTf_2]$ concentration increases is still observed, the data in this case show a temperature dependence much closer to linearity, though it should be noted that this linearity is potentially the result of the narrower temperate range measured for the anion and the VTF behaviour not being visible in this range. The anion diffusion coefficients below 293 K could not be resolved unlike the ^{1}H diffusion measurements that could be obtained down to 273 K. As a result these data were fitted to the Arrhenius, rather than VTF, equation, providing activation energies for the translational mobility of the anion. As can be seen from Table 3, this activation energy is strongly dependent on the $Na[NTf_2]$ concentration, doubling in size when the concentration is increased from 0.2 to 0.5 mol kg^{-1}. This is most likely a result of the stronger electrostatic interactions between this anion and the Na ions, compared with the larger IL cation. In the latter case the interaction between the anion and the positively charged nitrogen on the cation is sterically hindered by the large oligoether groups.

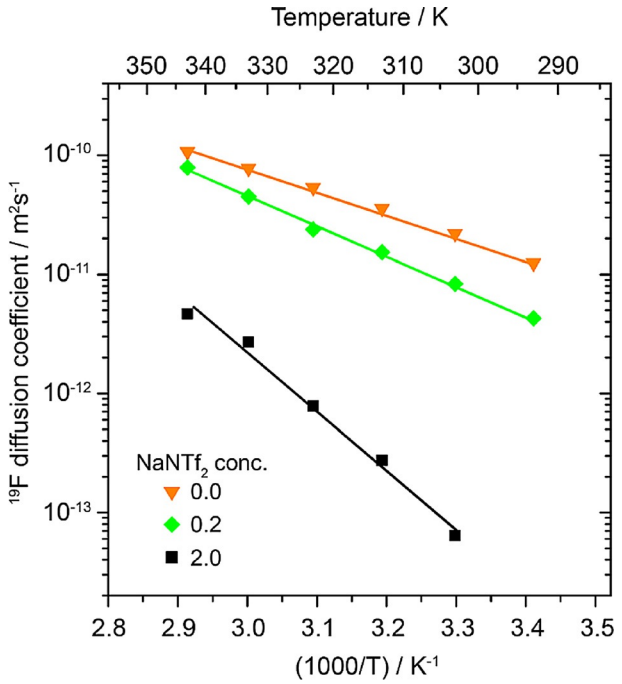

Figure 6. ^{19}F diffusion coefficients as a function of temperature for the pure IL and the lowest and highest $NaNTf_2$ concentrations (0.2 and 2.0 mol kg^{-1}). The error bars are contained within the size of the data points.

Table 3. Activation energies determined from the temperature-dependent ^{19}F diffusion coefficients via Arrhenius fits.

$NaNTf_2$ concentration [mol kg^{-1}]	E_A [kJ mol^{-1}]
0.0	34.4 ± 1.0
0.2	48.0 ± 1.2
0.5	94.3 ± 5.8

2.5. T_1 relaxation Measurements

To further quantify the variations in the dynamics of the different ionic species as a function of temperature and $Na[NTf_2]$ concentration, the ^{1}H, ^{23}Na and ^{19}F longitudinal NMR relaxation times (T_1s) were measured, and are shown in Figure 7. For several of the samples, the T_1 minima (at which the timescale for the dynamics is equal to the inverse of the nuclear Larmor frequency) were found to be within, or close to, the observed temperature range, allowing the data to be fitted using Bloembergen–Purcell–Pound (BPP) theory[40] [Eq. (3)]:

$$\frac{1}{T_1} = C\left(\frac{\tau_c}{1+\omega_0^2\tau_c^2}+\frac{4\tau_c}{1+4\omega_0^2\tau_c^2}\right) \quad (3)$$

In this expression, ω_0 is the Larmor frequency and τ_c is the correlation time for the dynamic process modulating the relevant relaxation mechanism. The factor C depends on the NMR interactions contributing to the relaxation. In the case of the ^{1}H and ^{19}F data, this was assumed to be homonuclear dipolar couplings, modelled in this case as a spin pair with $C=3d^2/10$ where d is the dipolar coupling constant, given by Equation (4):

$$d = -\frac{\mu_0}{4\pi}\frac{\gamma^2\hbar}{r^3} \quad (4)$$

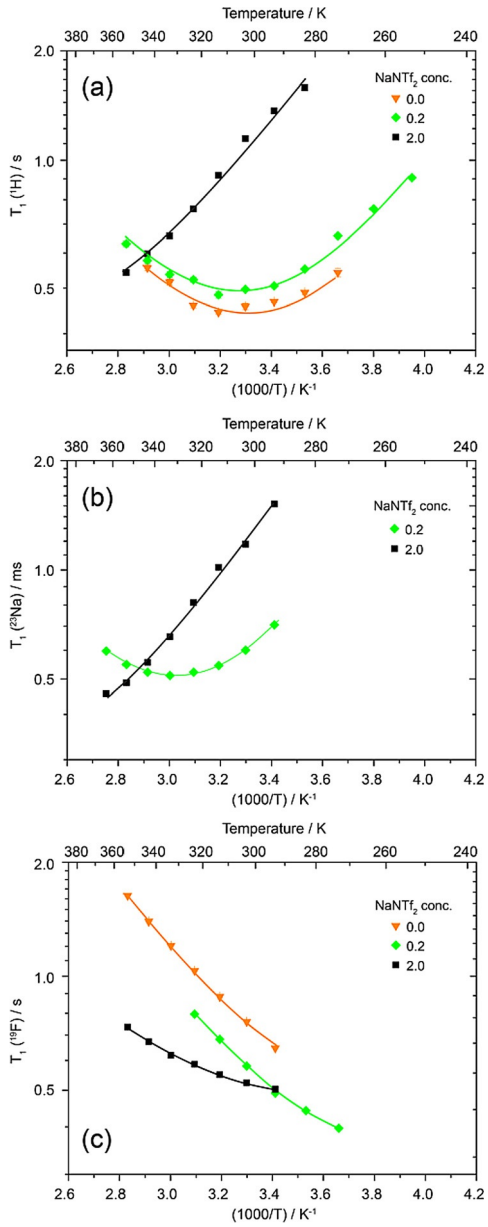

Figure 7. a) ^{1}H, b) ^{23}Na and c) ^{19}F T_1 relaxation times as a function of inverse temperature for the pure IL and the lowest and highest $NaNTf_2$ concentrations (0.2 and 2.0 mol kg^{-1}). The error bars are contained within the size of the data points. Lines show fits to BPP theory.

Here, μ_0 is the permeability of free space ($4\pi\times10^{-7}$ H m^{-1}), γ is the gyromagnetic ratio of the nucleus in question, $\hbar$ is the reduced Planck constant ($h/2\pi$) and r is the distance between the two coupled spins. The latter parameter was allowed to vary in the fitting of the ^{1}H and ^{19}F data. It should be noted that due to the low resolution of the ^{1}H NMR spectra, individual sites could not be resolved and thus the T_1 values represent an average over all sites. Since ^{23}Na is a quadrupolar nucleus, the quadrupolar interaction was assumed to be the dominant relaxation mechanism for this nucleus and the factor C was set as $4\pi^2\nu_Q^2$, where ν_Q is the quadrupolar coupling frequency in Hz.

The temperature-dependent ^{1}H T_1 relaxation times are shown in Figure 7a for the pure IL (0.0), the 0.2 and the 2.0 mol kg^{-1} $Na[NTf_2]$ concentrations. The T_1 minima for both the 0.0 and 0.2 mol kg^{-1} concentrations occur at a temperature of approximately 300 K. Fits of these data sets to BPP theory were carried out, and the resulting parameters are shown in Table 4. As expected given the similarity in the position of the T_1 minima for these two samples, the activation energies, dipolar coupling constants, and correlation times τ_c (at 300 K) are equal to within the uncertainty of the fit for these two samples (note that the correlation time can be considered as the time it takes for the cation to undergo a rotation through an angle of 1 radian). This similarity can be rationalised in terms of the molar ratio of the Na and $[N_{2(2O2O1)3}]$ cations, in this case approximately 1:9, meaning that most of the larger cations will experience an environment very similar to the pure IL.

Table 4. Fitting parameters for ^{1}H T_1 relaxation measurements [Eq. (3) with $C=3d^2/10$ where d is defined in Eq. (4)].

$NaNTf_2$ concentration [mol kg^{-1}]	E_A [kJ mol^{-1}]	D [kHz]	τ_c [300 K s^{-1}]
0.0	20.1 ± 2.0	43 ± 1	$(3.6\pm0.1)\times10^{-10}$
0.2	18.6 ± 1.5	40 ± 2	$(3.8\pm0.1)\times10^{-10}$
2.0	17.5 ± 1.5	42[a]	$(2.1\pm0.2)\times10^{-9}$

[a] Value restrained in fit.

For the 2.0 mol kg^{-1} $Na[NTf_2]$ concentration, the ^{1}H T_1 relaxation behaviour is significantly altered, with the minimum shifted to a much higher temperature. Similar behaviour has previously been reported by Bayley et al. where various diluents were used to enhance the mobility of lithium ions in $Li[NTf_2]$ and by Simons et al.[41] in which BPP fits showed monotonic slowing of anion dynamics with the addition of Zinc salt in $[C_4mpyr][dca]$ salt, indicative of increased cation/anion association. Due to the T_1 minimum being well outside of the observed range, the BPP fitting of this data required the dipolar coupling constant to be fixed at 42 kHz. The resulting activation energy is not significantly different to the other samples, however the correlation time is approximately an order of magnitude larger than for the 0.0 and 0.2 mol kg^{-1} $Na[NTf_2]$ concentrations (i.e., much slower rotation of the cation). This dramatic reduction in cation mobility is consistent with both the diffusion and conductivity results, and again suggests significant associations with the Na^+ ions that cause cross-linking between two or more IL cations.

The ^{23}Na T_1 measurements for the 0.2 and 2.0 mol kg^{-1} $Na[NTf_2]$ concentrations (Figure 7b, Table 5) show a similar trend to the ^{1}H T_1 data. The T_1 minimum occurs at a temperature of around 330 K for the lower $Na[NTf_2]$ concentration with activation energies similar to that measured for the larger cation. At the higher concentration the ^{23}Na T_1 minimum is shifted to a higher temperature, indicative of significantly reduced dynamics, and confirmed by a factor of 4 increase in the correlation time. Interestingly, the quadrupolar frequency

Table 5. Fitting parameters for ^{23}Na T_1 relaxation measurements [Eq. (3) with $C=4\pi^2\nu_Q^2$ where ν_Q is the quadrupolar frequency].

$NaNTf_2$ concentration [mol kg^{-1}]	E_A [kJ mol^{-1}]	ν_Q [kHz]	τ_c [300 K s^{-1}]
0.2	19.5 ± 1.0	170 ± 5	(1.6 ± 0.1) × 10^{-9}
2.0	18.5 ± 2.8	210 ± 25	(6.4 ± 1.3) × 10^{-9}

also changes, suggesting a difference in the average coordination environment of the Na^+ ions.

As evident from Figure 7c, the ^{19}F T_1 values show minima well below the experimental temperature range. The BPP fitting (Table 6) of these data sets provide correlations times at 300 K that are significantly lower than those of the cations. However, as for the cations, the anion correlation time is also seen to increase at higher $Na[NTf_2]$ concentrations, doubling on going from 0.2 to 2.0 mol kg^{-1}.

Table 6. Fitting parameters for ^{19}F T_1 relaxation measurements [Eq. (3) with $C=3d^2/10$ where d is defined in Eq. (4)].

$NaNTf_2$ concentration [mol kg^{-1}]	E_A [kJ mol^{-1}]	D [kHz]	τ_c [300 K s^{-1}]
0.0	16.0 ± 1.8	35 ± 3	(1.4 ± 0.5) × 10^{-10}
0.2	16.0 ± 1.0	42 ± 1	(1.3 ± 0.2) × 10^{-10}
2.0	12.5 ± 2.0	36 ± 3	(2.8 ± 0.4) × 10^{-10}

Taken together, the ^1H, ^{23}Na and ^{19}F activation energies and correlation times (at 300 K) for the 2.0 mol kg^{-1} concentration provide further evidence for strong associations between the Na and ammonium cations. The E_A values for ^1H and ^{23}Na are equal to within experimental uncertainty (ca. 18 kJ mol^{-1}), while that for the ^{19}F is significantly lower (12.5 kJ mol^{-1}). Moreover, the ^{19}F correlation times, being a measure of the reorientation rate of the CF_3 groups of the NTf_2 anions, are approximately an order of magnitude smaller than for the other two nuclei. This suggests that the mechanism causing the modulation of ^{23}Na quadrupolar couplings that dominates the relaxation of these nuclei is the same mechanism that causes the ^1H nuclei to relax, that is, the reorientation of the ammonium cation arms that modulates the ^1H–^1H dipolar couplings also alters the environment of the Na^+ cation. This association between the two cations could potentially be confirmed using through-space correlation NMR techniques such as ^1H–^{23}Na HOESY (heteronuclear Overhauser effect spectroscopy), but these have so far been unsuccessful in our laboratory due to the short ^{23}Na relaxation times.

2.6. Cyclic Voltammetry

The temperature dependence of the CV is presented in Figure 8 for the 3rd cycles of the 2.0 mol kg^{-1} $Na[NTf_2]$ at 323 K (Figure 8a) and 348 K (Figure 8b). Sodium metal deposition is evident at −2.2 V vs. $Fc|Fc^+$ with a corresponding stripping peak present at around −1.8 V. The highest $Na[NTf_2]$ concentration provided the most stable cycling, as previously reported by Forsyth et al.[23] The Na deposition and dissolution peaks remained the most stable upon cycling up to 10 cycles at 323 K. However the dissolution peak continued to drift towards more positive potentials with continued cycling indicating the presence of a strong SEI formed on the copper working electrode. Further electrochemical analysis is currently being performed, including the measurement of transference numbers, and will be reported elsewhere.

3. Conclusions

We have established the viability of designing an IL with ether-functionalised groups on a bulky quaternary ammonium cation to enhance the sodium solubility in an IL electrolyte for potential use as an electrolyte in a sodium-based electrochemical device. This approach has demonstrated the highly solvating nature of the ether groups to increase Na salt dissolution in an $[NTf_2]$ based electrolyte, enabling us to stably incorporate a high salt concentration of 2.0 mol kg^{-1} (57 mol%) Na into the $[N_{2(2O2O1)3}][NTf_2]$ electrolyte.

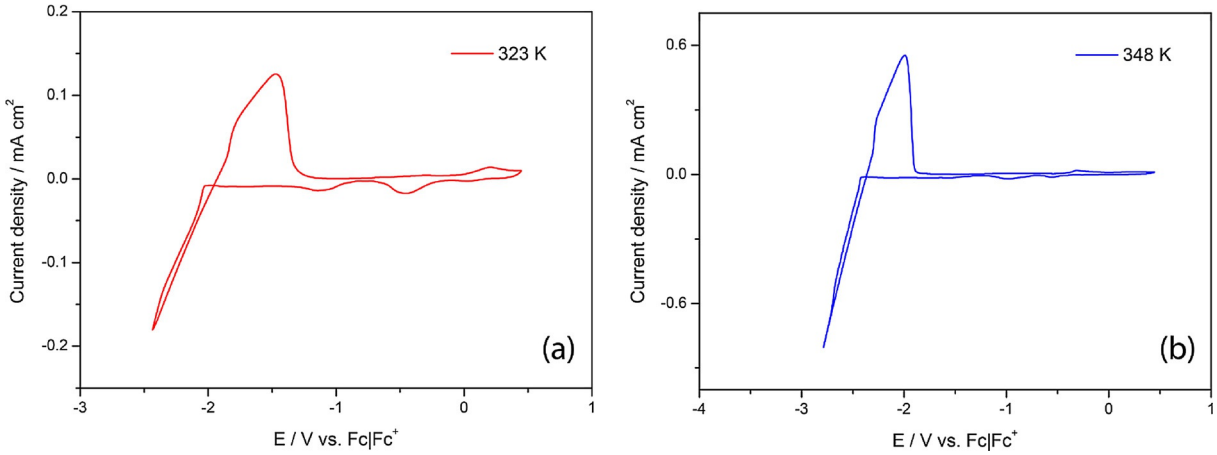

Figure 8. Cyclic voltammograms (3rd cycles) at a) 323 K and b) 348 K of the 2.0 mol kg^{-1} $Na[NTf_2]$ using a Cu working electrode and a Pt counter and reference electrode vs. $Fc|Fc^+$.

Increasing the Na ion concentration was found to decrease the ionic conductivity and self-diffusion coefficients, and increase the apparent viscosity and glass-transition temperature. NMR relaxation measurements suggest that this is largely related to the decreased mobility of the ions at higher salt concentrations. Interestingly the relaxation measurements also imply correlated dynamics between the IL cation and sodium, hinting at strong associations between these species and the possibility of Na cations acting as cross-links between multiple ammonium cations.

This IL electrolyte has demonstrated promising results as a candidate for future sodium device applications. Further work, including more comprehensive cyclic voltammetry and transference number measurements on this system is currently being conducted in our laboratory.

Acknowledgements

The ARC (Australian Research Council) is thanked for funding this work through the Discovery Projects (DP130101652) and Australian Laureate Fellowship programs (M.F. and D.R.M.) and for funding Deakin University's Magnetic Resonance Facility through LIEF grant LE110100141. The authors would also like to thank Dr Matthias Hilder and Dr Hyungook (Martin) Yoon for their contributions to this work. M.A. gratefully acknowledges Deakin University for travel funding through the „Thinker in Residence" program.

Keywords: diffusion · ionic conductivity · ionic liquids · NMR spectroscopy · sodium electrolytes

[1] M. Z. Jacobson, *Energy Environ. Sci.* **2009**, *2*, 148 – 173.
[2] D. R. MacFarlane, N. Tachikawa, M. Forsyth, J. M. Pringle, P. C. Howlett, G. D. Elliott, J. H. Davis, M. Watanabe, P. Simon, C. A. Angell, *Energy Environ. Sci.* **2014**, *7*, 232 – 250.
[3] S. A. Forsyth, J. M. Pringle, D. R. MacFarlane, *Aust. J. Chem.* **2004**, *57*, 113 – 119.
[4] D. R. MacFarlane, M. Forsyth, P. C. Howlett, J. M. Pringle, J. Sun, G. Annat, W. Neil, E. I. Izgorodina, *Acc. Chem. Res.* **2007**, *40*, 1165 – 1173.
[5] D. R. MacFarlane, J. M. Pringle, P. C. Howlett, M. Forsyth, *Phys. Chem. Chem. Phys.* **2010**, *12*, 1659 – 1669.
[6] J. B. Goodenough, *Energy Environ. Sci.* **2014**, *7*, 14 – 18.
[7] S.-M. Oh, S.-T. Myung, J. Hassoun, B. Scrosati, Y.-K. Sun, *Electrochem. Commun.* **2012**, *22*, 149 – 152.
[8] J. B. Goodenough, *Acc. Chem. Res.* **2013**, *46*, 1053 – 1061.
[9] C. Vidal-Abarca, P. Lavela, J. L. Tirado, A. V. Chadwick, M. Alfredsson, E. Kelder, *J. Power Sources* **2012**, *197*, 314 – 318.
[10] P. Thomas, D. Billaud, *Electrochim. Acta* **2002**, *47*, 3303 – 3307.
[11] C. R. Pope, K. Romanenko, D. R. MacFarlane, M. Forsyth, L. A. O'Dell, *Electrochim. Acta* **2015**, *175*, 62 – 67.
[12] A. Ferry, M. M. Doeff, L. C. DeJonghe, *Electrochim. Acta* **1998**, *43*, 1387 – 1393.
[13] A. Boschin, P. Johansson, *Electrochim. Acta* **2015**, *175*, 124 – 133.
[14] D. Monti, E. Jónsson, M. R. Palacín, P. Johansson, *J. Power Sources* **2014**, *245*, 630 – 636.
[15] C. Ding, T. Nohira, K. Kuroda, R. Hagiwara, A. Fukunaga, S. Sakai, K. Nitta, S. Inazawa, *J. Power Sources* **2013**, *238*, 296 – 300.
[16] C. Ding, T. Nohira, R. Hagiwara, K. Matsumoto, Y. Okamoto, A. Fukunaga, S. Sakai, K. Nitta, S. Inazawa, *J. Power Sources* **2014**, *269*, 124 – 128.
[17] S. A. M. Noor, P. C. Howlett, D. R. MacFarlane, M. Forsyth, *Electrochim. Acta* **2013**, *114*, 766 – 771.
[18] M. D. Slater, D. Kim, E. Lee, C. S. Johnson, *Adv. Funct. Mater.* **2013**, *23*, 947 – 958.
[19] L. Otaegui, E. Goikolea, F. Aguesse, M. Armand, T. Rojo, G. Singh, *J. Power Sources* **2015**, *297*, 168 – 173.
[20] A. Fukunaga, T. Nohira, Y. Kozawa, R. Hagiwara, S. Sakai, K. Nitta, S. Inazawa, *J. Power Sources* **2012**, *209*, 52 – 56.
[21] S. A. M. Noor, H. Yoon, M. Forsyth, D. R. MacFarlane, *Electrochim. Acta* **2015**, *169*, 376 – 381.
[22] H. Yoon, H. Zhu, A. Hervault, M. Armand, D. R. MacFarlane, M. Forsyth, *Phys. Chem. Chem. Phys.* **2014**, *16*, 12350 – 12355.
[23] M. Forsyth, H. Yoon, F. Chen, H. Zhu, D. R. MacFarlane, M. Armand, P. C. Howlett, *J. Phys. Chem. C* **2016**, *120*, 4276 – 4286.
[24] H. Yoon, P. C. Howlett, A. S. Best, M. Forsyth, D. R. MacFarlane, *J. Electrochem. Soc.* **2013**, *160*, A1629 – A1637.
[25] T. Tamura, K. Yoshida, T. Hachida, M. Tsuchiya, M. Nakamura, Y. Kazue, N. Tachikawa, K. Dokko, M. Watanabe, *Chem. Lett.* **2010**, *39*, 753 – 755.
[26] S. Terada, T. Mandai, R. Nozawa, K. Yoshida, K. Ueno, S. Tsuzuki, K. Dokko, M. Watanabe, *Phys. Chem. Chem. Phys.* **2014**, *16*, 11737 – 11746.
[27] M. Kar, B. Winther-Jensen, M. Forsyth, D. R. MacFarlane, *Phys. Chem. Chem. Phys.* **2014**, *16*, 10816 – 10822.
[28] M. Kar, B. Winther-Jensen, M. Forsyth, D. R. MacFarlane, *Phys. Chem. Chem. Phys.* **2013**, *15*, 7191 – 7197.
[29] M. Kar, B. Winther-Jensen, M. Armand, T. J. Simons, O. Winther-Jensen, M. Forsyth, D. R. MacFarlane, *Electrochim. Acta* **2016**, *188*, 461 – 471.
[30] K. Damodaran, *Ann. Rep. Nucl. Magn. Reson. Spec.* **2016**, *88*, 215 – 244.
[31] S. A. M. Noor, P. M. Bayley, M. Forsyth, D. R. MacFarlane, *Electrochim. Acta* **2013**, *91*, 219 – 226.
[32] T. Mandai, R. Nozawa, S. Tsuzuki, K. Yoshida, K. Ueno, K. Dokko, M. Watanabe, *J. Phys. Chem. B* **2013**, *117*, 15072 – 15085.
[33] M. P. Le, L. Cointeaux, P. Strobel, J.-C. Leprêtre, P. Judeinstein, F. Alloin, *J. Phys. Chem. C* **2012**, *116*, 7712 – 7718.
[34] A. R. Berens, I. M. Hodge, *Macromolecules* **1982**, *15*, 756 – 761.
[35] I. M. Hodge, A. R. Berens, *Macromolecules* **1982**, *15*, 762 – 770.
[36] F. M. Gray, *Solid Polymer Electrolytes*; VCH New York, **1991**.
[37] M. Galiński, A. Lewandowski, I. Stępniak, *Electrochim. Acta* **2006**, *51*, 5567 – 5580.
[38] K. Matsumoto, Y. Okamoto, T. Nohira, R. Hagiwara, *J. Phys. Chem. C* **2015**, *119*, 7648 – 7655.
[39] T. Reddy, *Handbook of Batteries*, McGraw-Hill Pub, **2002**.
[40] N. Bloembergen, E. M. Purcell, R. V. Pound, *Phys. Rev.* **1948**, *73*, 679 – 712.
[41] T. J. Simons, P. M. Bayley, Z. Zhang, P. C. Howlett, D. R. MacFarlane, L. A. Madsen, M. Forsyth, *J. Phys. Chem. B* **2014**, *118*, 4895 – 4905.

Manuscript received: June 27, 2016
Accepted Article published: August 4, 2016
Final Article published: August 17, 2016